Optics Letters

Second-harmonic focusing by a nonlinear turbid medium via feedback-based wavefront shaping

YANQI QIAO,[1,2] YAJUN PENG,[1,2] YUANLIN ZHENG,[1,2] FANGWEI YE,[1,2] AND XIANFENG CHEN[1,2,*]

[1]State Key Laboratory of Advanced Optical Communication Systems and Networks, Department of Physics and Astronomy, Shanghai Jiao Tong University, Shanghai 200240, China
[2]Key Laboratory for Laser Plasmas (Ministry of Education), Collaborative Innovation Center of IFSA (CICIFSA), Shanghai Jiao Tong University, Shanghai 200240, China
*Corresponding author: xfchen@sjtu.edu.cn

Received 22 March 2017; revised 4 April 2017; accepted 12 April 2017; posted 13 April 2017 (Doc. ID 291059); published 3 May 2017

Scattering has usually been considered detrimental for optical focusing or imaging. Recently, more and more research has shown that strongly scattering materials can be utilized to focus coherent light by controlling or shaping the incident light. Here, purposeful focusing of second-harmonic waves, which are generated and scattered from nonlinear turbid media via feedback-based wavefront shaping, is presented. This Letter shows a flexible manipulation of both disordered linear and nonlinear scattering signals, indicating more controllable degrees of freedom for the description of turbid media. This technique also provides a possible way to an efficient transmission of nonlinear signal at a desired location in the form of a focal point or other patterns. With the combination of random nonlinear optics and wavefront shaping methods, more interesting applications can be expected in the future, such as nonlinear transmission matrix, multi-frequency imaging, and phase-matching-free nonlinear optics.

OCIS codes: (190.2620) Harmonic generation and mixing; (160.3730) Lithium niobate; (290.4210) Multiple scattering; (110.0113) Imaging through turbid media.

https://doi.org/10.1364/OL.42.001895

Optical focusing and imaging through complex media has attracted much interest for its applications in biological tissue microscopy, since a feedback-based wavefront shaping method was proposed in 2007 [1–4]. Great progress has been made for complex imaging, perfect focusing, subwavelength focusing, and imaging in the last decade [5–9]. In fact, inelastic scattering light, especially nonlinear signal is also of great significance, such as focusing and imaging through turbid media via nonlinear feedback, as reported recently [10–12]. With a two-photon fluorescence feedback, spatiotemporal focusing, compression of chirped ultrashort pulses, and a noninvasive imaging method were demonstrated. With a nonlinear photoacoustic signal feedback, an enhanced optical focusing on a blood layer through a scattering medium was demonstrated. However, it is noticeable that the turbid media applied in previous studies are usually linear materials, which means no frequency conversion occurred directly during the scattering. Here, we demonstrated the manipulation of a second-order nonlinear signal (besides the linear part) generated and scattered from a turbid medium based on a wavefront shaping method, which indicates more controllable degrees of freedom (DOF) for describing the turbid medium. Future focusing and imaging through turbid media may profit from this technique.

A phase-matching (PM) or quasi-phase-matching (QPM) condition is required for high conversion efficiency in nonlinear optics, which may be hard to achieve in some cases [13]. In random nonlinear materials, a random QPM scheme was proposed, where the PM or QPM limitation can be loosened, and the conversion efficiency could increase linearly with the interaction length L [14–16]. When strong scattering is involved, L can be much larger than the sample size, but the emission signal will be totally divergent. For further investigation of the nonlinear optics inside the complex medium, a purposeful signal collecting way may be needed. Here, by manipulating the wavefront of the pump laser, we demonstrated an effective signal collecting way with the divergent nonlinear signal focused at an assigned location in the form of a point or other complex pattern.

In this Letter, the purposeful focusing of a second harmonic (SH) generated and scattered from superfine lithium niobate (LN) nanocrystal powder via feedback-based wavefront shaping method was demonstrated. The fundamental wave (FW) could also be focused using the same experimental setup via another round of optimization algorithm, as expected. We could restore FW and SH focus according to two different masks applied on the spatial light modulator (SLM). This technique provides more alternatives for future focusing and imaging applications. The SH focus size was detected around 380^2 nm^2 and the enhancement factor was estimated to be 27. More complex manipulations of the divergent signal, such as two SH foci and an SH focal line, were also demonstrated in the same experimental setup via some modified algorithms.

The concept of SH focusing via feedback-based wavefront shaping is shown in Fig. 1. Without shaping, the SH signals generated and scattered from the nonlinear turbid medium were divergent and manifested themselves as disorganized speckles on the screen [Fig. 1(a)]. An SH focal spot would be found forwardly or backwardly via an appropriate SLM

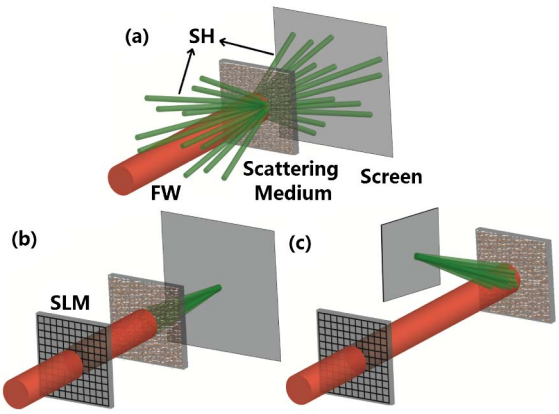

Fig. 1. Concept of focusing SH signals generated and scattered from a nonlinear medium via wavefront shaping. (a) Without shaping, the divergent SH signals form a disordered speckle pattern on the screen. With an appropriate SLM phase mask applied before the scattering medium, an SH focal point can be generated (b) forwardly or (c) backwardly on the screen.

mask generated from an optimization algorithm [Figs. 1(b) and 1(c)]. The SH wavefront is completely dependent on the fundamental wave and can be transiently manipulated by shaping the FW via SLM. Thus, the SH focusing is directly linked to the optimized wavefront of the FW.

The experimental setup is illustrated in Fig. 2. The light source was a high-energy diode-pumped all-solid-state *Q*-switched laser at the wavelength of 1064 nm (10 ns, 1 kHz). A half-wave plate and a Glan–Taylor polarizer were used for polarization and power control. The SLM had a resolution of 512×512 pixels, each with a rectangular area of $19.5\ \mu m^2 \times 19.5\ \mu m^2$. The FW was spatially filtered and expanded to fit the SLM aperture. Then the shaped wave was illuminated into the sample by an objective (40×, NA = 0.65, 160/0.17) after a dichroic mirror. The generated and scattered SH signal was collected in the reflected direction and imaged on a multi-spectral two-channel charge-coupled device (CCD) camera (JAI, AD-080 GE) by a lens after passing an attenuator and a filter. The CCD camera had a resolution of 1024×768 pixels, each with a rectangular area of $4.65\ \mu m^2 \times 4.65\ \mu m^2$. The magnification of the detection system was 25×. It is worth mentioning that the reflection configuration used here manipulates the backward signals instead of the forward ones, as shown in the transmission configuration in Fig. 1, which does not compromise the main claim of this Letter.

Here, LN nanocrystal powder was used as the second-order nonlinear scattering medium, which was prepared by the solid state reaction method using niobium pentoxide and lithium acetate dihydrate as reactants [17]. Then the electrophoresis method was applied to deposit the powder onto an indium-tin oxide (ITO)-coated glass substrate [18]. The LN particles had a maximum size of ~400 nm (see Fig. 2 inset), and the powder layer had a dimension of $30\ mm^3 \times 30\ mm^3 \times 0.1\ mm^3$. The scattering mean free path of the LN powder layer was estimated to be $l \cong 1.1\lambda$ for 532 nm of light from a coherent backscattering experiment [19–21].

The SH intensity at one single CCD pixel was recorded and served as a feedback to optimize the SLM phase mask. A genetic algorithm was applied to realize the optimization for its robustness to the noisy environments [22]. During the optimization, 512×512 pixels on the SLM were divided into 64×64 segments to reshape the FW wavefront. To start with, 100 masks were generated randomly as the first generation. Then they ranked according to the SH intensity at the target. With a higher rank, the mask has a higher chance to be selected as the parent to create the next generation, which contains another 100 masks. 10% ~ 30% mutation was applied into the creation, which means some segments of the mask randomly changed in the next generation. Next, the genetic process was repeated, and the latter generation would generally do better than the former, which indicated an optimization or a manipulation process of the divergent SH signals. Finally, a focal point or other desired patterns was formed.

Before manipulating the SH signals, we switched the CCD camera to an infrared channel and used a long-pass filter to check the system. Although the FW reflected from the dichroic mirror was relatively weak, it was still intense enough for CCD detection. After several generations of optimization, an FW focus was observed on the screen. Figures 3(a) and 3(b) show the

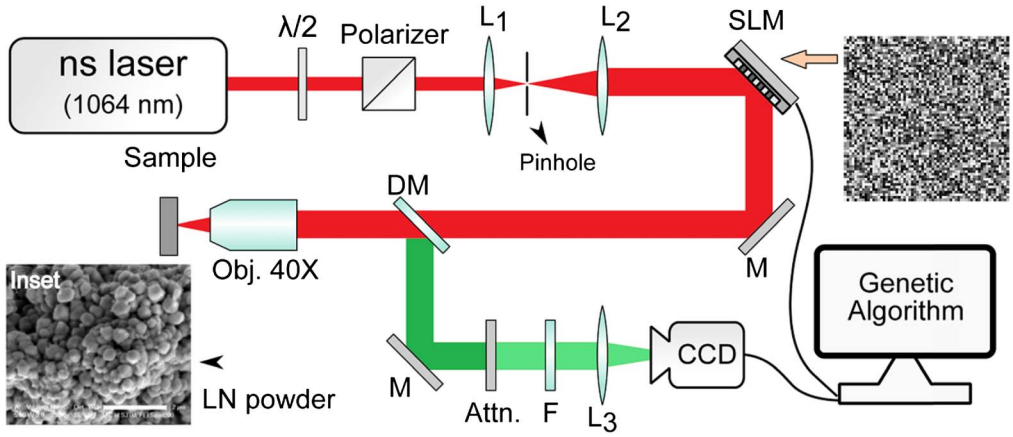

Fig. 2. Experimental setup for SH manipulation via wavefront shaping. $\lambda/2$, half-wave plate; L_{1a3}, lens; $f_{1a3} = 50$, 200, and 100 mm, respectively; M, mirror; DM, dichroic mirror; SLM, spatial light modulator; Attn., attenuator; F, filter. Inset: a scanning electron microscopy image of the LN powder, deposited onto an ITO-coated glass substrate (scale bar, 2 μm).

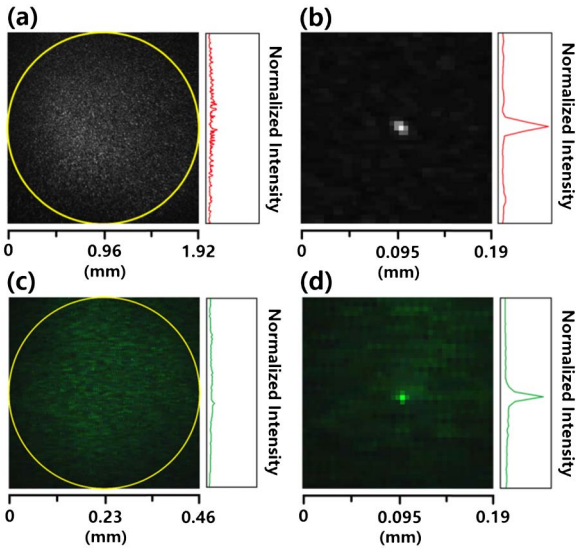

Fig. 3. (a), (c) Before optimization, the FW and SH speckle patterns have a size of around 2.9 and 0.65 mm^2 on the CCD, respectively. (b), (d) After optimization, these speckle patterns turn into focal points. The real SH focus size is estimated to be 380^2 nm^2.

detected FW patterns before and after optimization, respectively. The yellow circle marked the original speckle size to be around 2.9 mm^2. The optimized focus is around several pixels in size. This process was fast and repeatable, which confirmed the feasibility and stability of our system. When considering the SH signals, we switched the CCD camera to a visible channel and used a short-pass filter, as illustrated in Fig. 2. The SH speckle before optimization was disordered and had a profile size around 0.65 mm^2, as shown in Fig. 3(c). After optimization, an SH focus with about two pixels size was achieved, related to a real size around 380^2 nm^2. This result indicated an accurate location and a high resolution of the SH focus. It is worth mentioning that these foci could be reproduced after cutting off the SLM for a long time, via applying these optimized masks again.

Theoretically, there are two possible reasons for the SH focus. The one is that after optimization, the FW energy was focused onto the surface of a sample, and a point SH source was formed to emit SHG with relatively high energy. The other is that the FW energy was not focused, but the randomly scattered SH signals were focused outside the surface. In fact, we did not find FW focus (which should be much stronger) when we manipulated the SH focus in our experiment, so the former reason seems to be impossible. In addition, the real focus size is around 380^2 nm^2, indicating the multiple scattering plays an important role during the optimization, leading to a possibly perfect-focusing process [7].

The enhancement factor η of the SH focus was detected with the generation number at the target before and after optimization. As expected, η increased generally with the generation number until saturation, which was usually a local maximum value for genetic algorithm, instead of a global maximum value compared to other algorithms [22,23]. A typical enhancement in our SH experiments was estimated to be 27 after 300 generations, as shown in Fig. 4.

Some typical results of complex manipulations of the scattered SH signals were shown in Fig. 5. First, the average

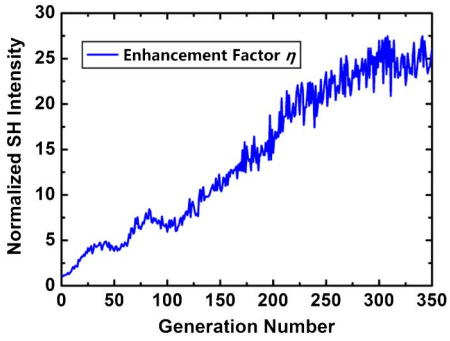

Fig. 4. Enhancement factor η of the normalized SH intensity at the target location versus the generation number. A typical value was estimated to be 27 after 300 generations.

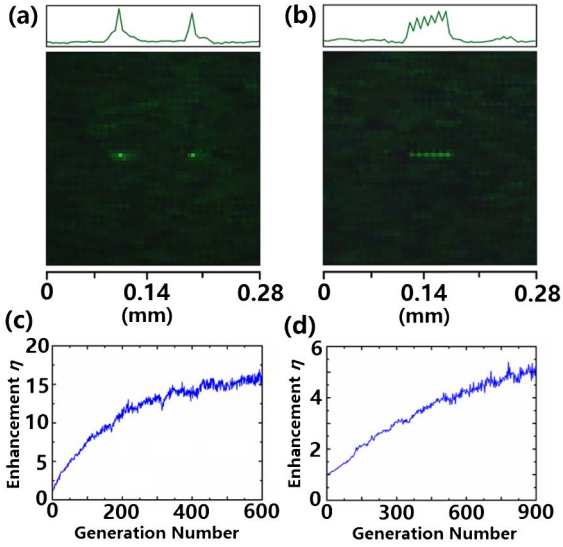

Fig. 5. (a) Two SH foci obtained on the CCD screen after approximate 600 generations. (b) Focal line formed on the screen after optimization, with a length about 2.2 μm. (c), (d) Enhancement factors of the two foci ($\eta \approx 15$) and the focal line ($\eta \approx 5$), respectively.

intensity of two assigned locations served as the feedback. After around 600 generations, two obvious SH foci were observed on the CCD screen, as shown in Fig. 5(a). The point-to-point distance is 3.7 μm. Similarly, if the average intensity of a series of pixels was set as the feedback, we would manipulate a focal line with a length of 2.2 μm, as shown in Fig. 5(b). The enhancement factors of these optimizations were estimated to be 15 and 5, respectively, as shown in Figs. 5(c) and 5(d).

In fact, the more complex manipulation we hope, the more time (generations) was needed and the lower the enhancement could be achieved based on our experiments. It is expected that any complex manipulation was theoretically possible. The flexible manipulation of the SH signals also indicates a simpler way to generate nearly arbitrary designed nonlinear patterns, compared to no-feedback-based wavefront shaping and domain design methods [24–29].

In our experimental design, LN nanoparticle powder was chosen for its large second-order susceptibility and high

refractive index ($n \approx 2.2$) for multiple scattering [13]. The maximum size of the particle was around 400 nm, which is smaller than the coherent interaction length L_c in a LN crystal. [L_c(532 nm) is about several microns.] This fact ensures that every single particle serves as an SH source and emits maximum signals [14]. Other nonlinear scattering materials, such as cubic boron nitride nanoparticles or porous nonlinear materials, are believed to be applicative in the same experiments. Other nonlinear processes, such as third-harmonic generation, three-wave mixing, and coherent anti-Stokes Raman scattering are also expected to behave similarly with proper configurations [13]. However, there are some main limitations for this method on the future applications, such as the optimization speed and enhancement factor when manipulating complex patterns. For example, it took ~10 min of optimization to get the SH focal line in our experiment. These problems are believed to be solved with faster software-hardware configuration, better samples, and proper algorithms in the future [22,23,30].

In conclusion, we have reported the purposeful focusing of SH generated and scattered from superfine LN nanocrystal powder via feedback-based wavefront shaping method. A genetic algorithm was applied in the optimization for its robustness. The FW and SH foci could be restored, respectively, according to the masks applied on the SLM by optimization. The SH focal spot in our experiment had a size of around 380^2 nm^2, and the enhancement factor was estimated to be 27 after 300 generations. Besides, more complex manipulations of the scattered SH signals were demonstrated, such as two SH foci and a focal line. Other nonlinear scattering materials or nonlinear processes are believed to behave similarly under proper configuration.

This Letter indicates more controllable DOF for the description of turbid media. In fact, the transmission matrix (TM) method was very popular in describing the scattering properties of linear media [31,32]. Image recovery through scattering media becomes possible and easy based on this method, except that the sample needs to be very stable in a certain time interval [33,34]. With nonlinear scattering media, a nonlinear TM may be expected and future focusing and imaging through turbid media may profit from this expansion. A point spread function method is also effective in describing scattering media for a high-speed color imaging, besides the TM method, which may be applied in the nonlinear medium and nonlinear imaging [35]. This technique also provides a possible way to transmit an efficient nonlinear signal at a desired location in the form of a point or other patterns. With this combination of random nonlinear optics and wavefront shaping method, more and more interesting applications can be envisioned in the future, such as multi-frequency imaging and phase-matching-free or domain-design-free nonlinear optics.

Funding. National Natural Science Foundation of China (NSFC) (11421064, 61235009).

Acknowledgment. The authors thank Dr. Haigang Liu for his help with the experiment.

REFERENCES

1. I. M. Vellekoop and A. P. Mosk, Opt. Lett. **32**, 2309 (2007).
2. I. M. Vellekoop and A. P. Mosk, Phys. Rev. Lett. **101**, 120601 (2008).
3. I. M. Vellekoop, Opt. Express **23**, 12189 (2015).
4. R. Horstmeyer, H. Ruan, and C. Yang, Nat. Photonics **9**, 563 (2015).
5. D. B. Conkey and R. Piestun, Opt. Express **20**, 27312 (2012).
6. A. P. Mosk, A. Lagendijk, G. Lerosey, and M. Fink, Nat. Photonics **6**, 283 (2012).
7. I. M. Vellekoop, A. Lagendijk, and A. P. Mosk, Nat. Photonics **4**, 320 (2010).
8. J. H. Park, C. Park, H. Yu, J. Park, S. Han, J. Shin, S. H. Ko, K. T. Nam, Y. H. Cho, and Y. Park, Nat. Photonics **7**, 454 (2013).
9. C. Park, J. H. Park, C. Rodriguez, H. Yu, M. Kim, K. Jin, S. Han, J. Shin, S. H. Ko, K. T. Nam, Y. H. Lee, Y. H. Cho, and Y. Park, Phys. Rev. Lett. **113**, 113901 (2014).
10. O. Katz, E. Small, Y. Bromberg, and Y. Silberberg, Nat. Photonics **5**, 372 (2011).
11. O. Katz, E. Small, Y. Guan, and Y. Silberberg, Optica **1**, 170 (2014).
12. P. Lai, L. Wang, J. W. Tay, and L. V. Wang, Nat. Photonics **9**, 126 (2015).
13. R. W. Boyd, *Nonlinear Optics* (Academic, 2008).
14. M. Baudrier-Raybaut, R. Haidar, P. Kupecek, P. Lemasson, and E. Rosencher, Nature **432**, 374 (2004).
15. R. Fischer, S. M. Saltiel, D. N. Neshev, W. Krolikowski, and Y. S. Kivshar, Appl. Phys. Lett. **89**, 191105 (2006).
16. S. Stivala, A. C. Busacca, A. Pasquazi, R. L. Oliveri, R. Morandotti, and G. Assanto, Opt. Lett. **35**, 363 (2010).
17. T. T. Su, H. Jiang, H. Gong, and Y. C. Zhai, Cryst. Res. Technol. **45**, 977 (2010).
18. B. S. Jeon, J. S. Yoo, and J. D. Lee, J. Electrochem. Soc. **143**, 3923 (1996).
19. M. P. Van Albada and A. Lagendijk, Phys. Rev. Lett. **55**, 2692 (1985).
20. P. E. Wolf and G. Maret, Phys. Rev. Lett. **55**, 2696 (1985).
21. P. C. de Oliveira, A. E. Perkins, and N. M. Lawandy, Opt. Lett. **21**, 1685 (1996).
22. D. B. Conkey, A. N. Brown, A. M. Caravaca-Aguirre, and R. Piestun, Opt. Express **20**, 4840 (2012).
23. I. M. Vellekoop and A. P. Mosk, Opt. Commun. **281**, 3071 (2008).
24. Y. Q. Qin, C. Zhang, Y. Y. Zhu, X. P. Hu, and G. Zhao, Phys. Rev. Lett. **100**, 063902 (2008).
25. T. Ellenbogen, N. Voloch-Bloch, A. Ganany-Padowicz, and A. Arie, Nat. Photonics **3**, 395 (2009).
26. A. Shapira, R. Shiloh, I. Juwiler, and A. Arie, Opt. Lett. **37**, 2136 (2012).
27. X. H. Hong, B. Yang, C. Zhang, Y. Q. Qin, and Y. Y. Zhu, Phys. Rev. Lett. **113**, 163902 (2014).
28. H. Liu, J. Li, X. Zhao, Y. Zheng, and X. Chen, Opt. Express **24**, 15666 (2016).
29. H. Liu, J. Li, X. Fang, X. Zhao, Y. Zheng, and X. Chen, Opt. Express **24**, 24137 (2016).
30. A. S. Hemphill, J. W. Tay, and L. V. Wang, J. Biomed. Opt. **21**, 121502 (2016).
31. C. W. J. Beenakker, Rev. Mod. Phys. **69**, 731 (1997).
32. S. M. Popoff, G. Lerosey, R. Carminati, M. Fink, A. C. Boccara, and S. Gigan, Phys. Rev. Lett. **104**, 100601 (2010).
33. S. Popoff, G. Lerosey, M. Fink, A. C. Boccara, and S. Gigan, Nat. Commun. **1**, 1 (2010).
34. S. M. Popoff, G. Lerosey, M. Fink, A. C. Boccara, and S. Gigan, New J. Phys. **13**, 123021 (2011).
35. H. Zhuang, H. He, X. Xie, and J. Zhou, Sci. Rep. **6**, 32696 (2016).